Comparison of Experimental and Theoretical Heterogeneous Nucleation on Ultrafine Carbon Particles

Doh-Won Lee,[†] Philip K. Hopke,*[,†] Don H. Rasmussen,[†] Hwa-Chi Wang,[‡,§] and Rashid Mavliev[‡]

Clarkson University, Potsdam, New York, Illinois Institute of Technology, Chicago, Illinois, and Air Liquide, Chicago Research Center, Countryside, Illinois

Received: December 24, 2002; In Final Form: September 28, 2003

Using a modified turbulent mixing CNC, the heterogeneous nucleation of different compounds (working fluids) on nanometer sized carbon particles was examined. The working fluids were dibutyl phthalate, octadecane, octadecanol, and octadecanoic acid. Based on the particle size distributions measured with a scanning mobility particle sizer system, nucleation and consequent growth were examined with respect to different temperature and vapor pressure for each working fluid. Nucleation rates for all conditions were calculated from the fitted size distribution data by subtracting the residual nonactivated particle concentration for each condition. Experimental nucleation rates were compared to the calculated ones based on Fletcher's heterogeneous nucleation theory. This theory matches well with the experiments with octadecanol and octadecanoic acid, and at high supersaturation ratios for dibutyl phthalate. However, the theory shows discrepancies with the observed phenomena at low supersaturation for dibutyl phthalate, and especially for octadecane. Several possible hypotheses for the discrepancies and observed particle growth are discussed.

1. Introduction

Attention has now focused on the ultrafine fraction of the ambient aerosol. Ultrafine particles have been proposed as a major factor contributing to the adverse health effects of particulate air pollution.[1,2] To characterize these ultrafine particles, systems have been developed in which the particles are nucleated with water vapor and grown to sizes where they can collected by inertia.[3−5] Thus, understanding heterogeneous nucleation becomes more important.

Although possible formation mechanisms for these small particles are discussed in the literature, complete theoretical models are not yet available. One main reason for the complexity of the atmospheric system. Any simplified description can only be proposed based on a solid experimental foundation. However, limited experimental methods are available to investigate particle formation processes, even in model systems.

Prior to developing better theoretical models through ideal experiments, measurements of the nucleation behavior of model compounds onto carbon particles were performed to examine the relationship between molecular properties of the condensing vapor (working fluid) and the particles. The experimental results were converted to experimental nucleation rates for the comparison with the ones calculated with well-known Fletcher's heterogeneous nucleation theory.[6] In this paper, the results of such experiments are presented along with several hypotheses introduced to explain the discrepancies between the experiment and the theory. These hypotheses may enhance current limited theoretical understanding of heterogeneous nucleation described in the next section and provide useful insights into the nature of the processes involved.

[†] Clarkson University.
* Corresponding author. Fax: 315 268 4410. E-mail: hopkepk@clarkson.edu
[‡] Illinois Institute of Technology.
[§] Air Liquide.

2. Theoretical Background

There has been continued interest in developing an accurate nucleation theory since the early work of Volmer and Weber.[7] According to Wu,[8] Volmer[9] defined the simplest model for the heterogeneous nucleation with the assumption that impurity surfaces permit liquid cluster growth as spherical caps with constant wetting angle θ (Figure 1).

In most cases, the surface of the substrate should not be considered to be flat. It should be treated as a convex surface, especially for nanometer size heterogeneous nuclei. The Gibbs free energy for heterogeneous nucleation is expressed as

$$\Delta G = \left(\frac{\mu_l - \mu_g}{\Omega}\right)V_l + \gamma_{gl}A_{gl} + (\gamma_{ls} - \gamma_{gs})A_{ls} \qquad (1)$$

in which μ_l and μ_g are, respectively, the chemical potential of the liquid and gas phase, Ω is the average volume per monomer in the bulk liquid, V_l is the liquid volume, γ_{ij} is the macroscopic surface energy per unit area of $i-j$ interface, and A_{ij} denotes the interfacial surface area of the $i-j$ interface, respectively. Referring to Figure 2

$$V_l = \frac{1}{3}\pi r^3(2 - 3\cos\psi + \cos^3\psi) - \frac{1}{3}\pi a^3(2 - 3\cos\varphi + \cos^3\varphi)$$

$$A_{gl} = 2\pi r^2(1 - \cos\psi) \qquad (2)$$

$$A_{ls} = 2\pi a^2(1 - \cos\varphi)$$

and

$$\cos\psi = -(r - a\cos\theta)/d = -(r - am)/d$$

$$\cos\varphi = (a - r\cos\theta)/d = (a - rm)/d \qquad (3)$$

10.1021/jp0278216 CCC: $25.00
Published on Web 11/07/2003

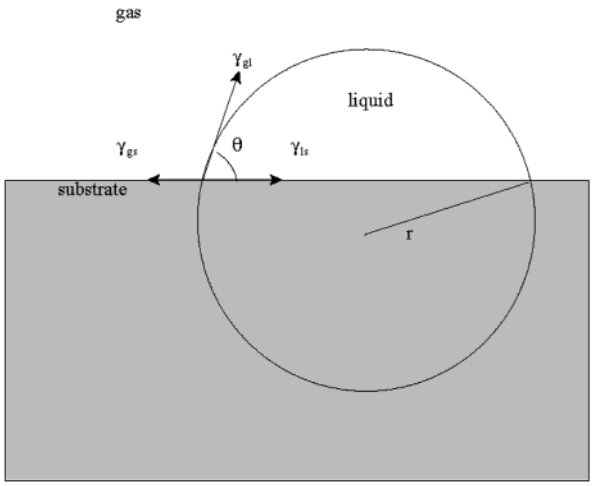

Figure 1. Spherical cap model for heterogeneous nucleation. The contact angle θ is determined by force balance of the surface tension γ between the gas, liquid, and the substrate. The term r is the radius of the projected sphere.

where $d = (a^2 + r^2 - 2arm)^{1/2}$ with $m = \cos\theta = (\gamma_{gs} - \gamma_{ls})/\gamma_{gl}$.The symbols, r and a, used in eqs 2 and 3 are the radii of the condensing cluster and the heterogeneous nuclei particle, respectively.

Setting $\partial G/\partial r = 0$ and solving the resulting eq 1 in combination with the eqs 2 and 3, Fletcher[6] showed that the equation for the critical radius r^* is

$$r^* = -2\gamma_{gl}/\Delta G_v \tag{4}$$

where ΔG_v is $-k_B T \ln S/\Omega$, in which k_B is the Boltzmann constant, T is temperature, and S is the supersaturation ratio, $S = P/P_{sat}(T)$, the actual pressure of the monomer divided by its equilibrium vapor pressure at the temperature of interest. Substituting eqs 2−4 into eq 1 and letting $x = a/r^*$, Fletcher[6] obtained the equation for the Gibbs free energy of formation of a critical embryo:

$$\Delta G^* = \frac{8\pi\gamma_{gl}^{\ 3}}{3(\Delta G_v)^2} f(m.x) \tag{5}$$

where

$$f(m,x) = 1 + \left(\frac{1-mx}{g}\right)^3 + x^3\left\{2 - 3\left(\frac{x-m}{g}\right) + \left(\frac{x-m}{g}\right)^3\right\} + 3mx^2\left(\frac{x-m}{g} - 1\right) \tag{6}$$

with $g = (1 + x^2 - 2mx)^{1/2}$.

At and above the given S, the (preexisting) heterogeneous nucleus particle, having radius of a, can have enough condensable monomers adsorbed on the surface to form a stable critical cluster, which is the process of heterogeneous nucleation. Below the given S, fewer monomers can also be deposited to form a cluster, but these monomers will evaporate eventually because the decrease in free energy on association of these monomers is not sufficient to overcome the surface energy barrier to form the critical cluster. At a given S, particles having size of "a" or larger are activated by heterogeneous nucleation and then undergo growth by condensation of more monomers onto this critical cluster, while particles having a radius smaller than "a" in size are not activated and the monomers deposited on the surfaces eventually evaporate back to the gas phase.

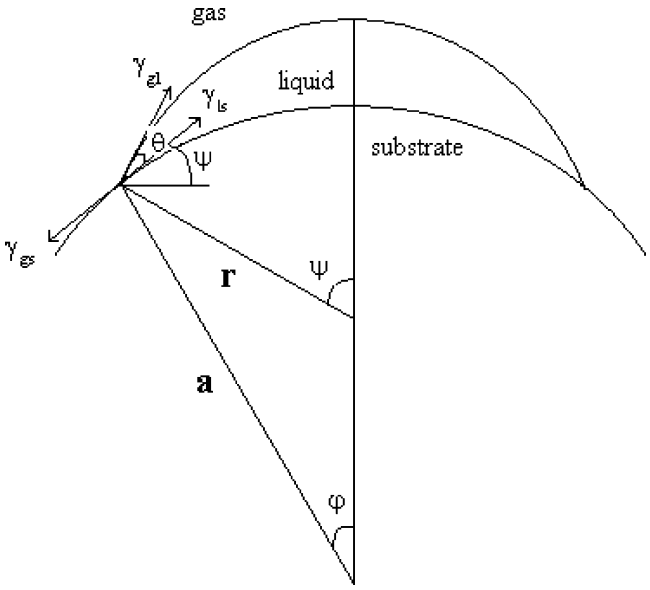

Figure 2. Schematic representation of a liquid cluster on a spherical aerosol particle: r, cluster radius; ψ, contact angle; and a, radius of the spherical aerosol particle.

To calculate the nucleation rate, classical theory involves several assumptions. First, it assumes that only a single monomer is added to or removed from the cluster in each step of the growth and evaporation process. The next assumption is that the sticking coefficient is 1, so that the impingement rate is the number of collisions between monomers and an n-mer per unit time. Next, for the evaporation rate, the constrained equilibrium hypothesis is applied, which asserts that the metastable gas-phase obeys the laws of fluctuation thermodynamics.[8] With the boundary condition that there is no monomer depletion, the steady-state nucleation rate, J, for the critical cluster is calculated by the steepest descent approximation. The resulting equation[8] for this convex spherical surface case is

$$J \approx \frac{s(\theta)}{\sqrt{v(\theta)}} \sqrt{\frac{2\Omega^2\gamma}{\pi m_1}} f_{1\,het} f_1 \{1 + (n^*_{hom})^{-1/3}\}^2 \exp\left(\frac{-\Delta G^*}{k_B T}\right) \tag{7}$$

where $s(\theta) = (1 - \cos\theta)/2$ and $v(\theta) = V_l/(4\pi r^3/3)$, in which $s(\theta)$ and $v(\theta)$ are, respectively, the exposed surface and volume ratios relative to an entire projected sphere, γ is the macroscopic surface energy per unit area at the liquid−gas interface, m_1 is the mass of a monomer, f_1 is the monomer concentration in the gas, $f_{1\,het}$ is the number concentration of existing nuclei, and the factor of $(1 + n^{*-1/3}_{hom})^2$ accounts for treating an n^*-mer as a sphere rather than a flat surface.

The interactions between the nuclei and vapor molecules are likely to have a strong influence on the heterogeneous nucleation process. The formation energy of the working fluid embryo will involve the interaction of solid−liquid and liquid−gas interfaces. According to Fletcher,[10] one of the most important parameters in this case is the contact angle between the particle surface and the condensed phase. However, the contact angle for nanometer-sized particles is not available and the contact angle of bulk material may not be valid. White[11] found appreciable differences between microscopic and macroscopic contact angles.

In addition to physical characterization, chemical characterization is the key to determining the role of the different particle formation processes as stated by Friedlander and Lippmann.[12] When nanometer-sized particles are of concern, near molecular

scale chemical interactions probably need to be considered. Very little information is available in the literature. Helsper and Niessner[13] investigated the effect of the vapor substance on the behavior of an expansion-type CNC for two working fluids, water and butanol. They found that two particle substances, Ag and NaCl, did not affect the Kelvin diameter when butanol was used as the working fluid. However, the size of NaCl particles was overestimated by 2.5 times when water was used. Similar results were found by Porstendörfer et al.[14] Kesten et al.[15] found different detection efficiency of the TSI CNC 3025 with butanol as a working fluid for NaCl and Ag particles. Kousaka et al.[16] found smaller, but still different results for NaCl and Ag particles. The brief description of results by Madelaine and Metayer[17] showed differences in CNC sensitivity for NaCl, V_2O_5, and H_2SO_4 particles. The state of theoretical understanding is very limited and, therefore, experimental investigation of the effects of the nuclei composition on nucleation activation become important.

These preliminary works suggest the influence of nucleus composition and working fluid vapor. However, there is insufficient and inconsistent data for establishing a complete theoretical description of the phenomena.

3. Experimental Setup

The basic components of the experimental system are a combustion chamber for carbon particle generation, a TMCNC for heterogeneous nucleation, and a differential mobility analyzer (DMA) and a conventional condensation nuclei counter (CNC) together for particle size distribution measurements. The TMCNC employed is the same one used in the study of Hopke et al.[18] and Mavliev et al.[19] More detailed information is given in the following subsections.

Particle Generation. Carbon particles, which are used as existing nuclei for the heterogeneous nucleation, were generated by a combustion process. The method is same as described in Lee,[20] and is similar to that of Li and Hopke.[21] The particles were produced by burning natural gas using a Bunsen burner. Filtered clean dilution air was introduced to keep the generated particles from coagulating in the chamber. The minimum particle size generated in the combustion process is not known, and particles smaller than 6 nm (see next section) were not observable but are presumed present. The generated and measured carbon particles on average had a geometric mean of 9.9 nm with geometric standard deviation (GSD) of 1.33. The average concentration of the carbon particles at the mean diameter is about 225 particles/cm^3, equivalent to 7175 particles/cm^3 as d*N*/dlogDp at that particle size.

Heterogeneous Nucleation. To examine the heterogeneous nucleation, a modified TMCNC[16,17] was used. As shown in Figure 3, the TMCNC consists of three parts: saturator, mixer, and condenser. All three parts of TMCNC are machined from blocks of aluminum alloy that allows uniform temperature distribution within the block. An outer Teflon shell provides insulation for heated parts.[16] The temperatures of the heated parts are controlled separately by a circuit board and a data acquisition system (5500MF from ADAC corp.) with an accuracy of ±0.2 °C while the temperature of condenser was maintained at 20 °C by a circulating water bath. A digital thermometer (model HH 12 from OMEGA Engineering, Inc.) was used as an additional reference for the temperature.

The TMCNC has two chambers of equal size in the saturator. Flows from these two chambers are connected before passing through the mixer in Figure 3. One saturator chamber (so-called "wet" chamber) can be filled with 15−20 cm^3 by volume of a working fluid while the other chamber ("dry") is kept dry, but at the same temperature.[16,17] The degree of supersaturation is changed by varying the ratio of flows passing through these two chambers while maintaining a constant total flow.

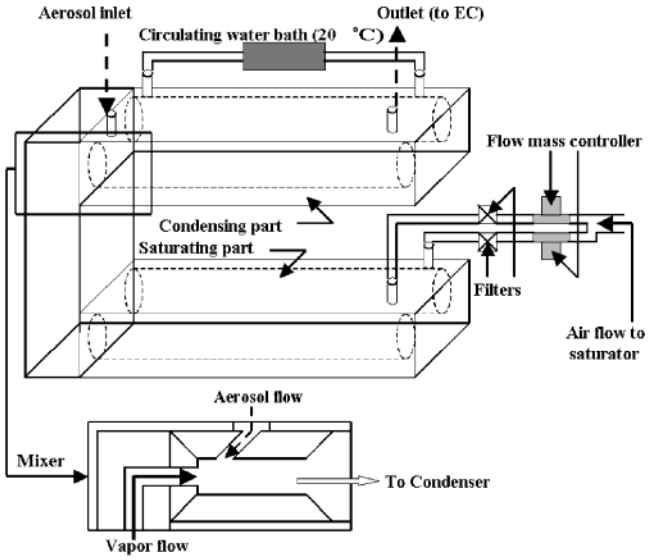

Figure 3. Schematic diagram of the modified TMCNC.

After these two coaxial flows are turbulently mixed in the mixer, they are then directed to the condenser. The residence time of particles in the condensation tube is about 2 s at a flow rate of 1.4 lpm. The actual residence time may be somewhat shorter because of the turbulent jet flow structure at the entrance of the condenser. However, it is sufficient for particle growth.[28]

By changing the flow ratio as well as temperature of the saturator, the TMCNC produces different supersaturation ratios. The flow rate coming from the saturator was 0.4 lpm, which results 1.4 lpm of flow to the DMA with the aerosol stream of 1.0 lpm. The wet flow and dry flow out of 0.4 lpm of saturator flow are controlled by two flow mass controllers as shown in Figure 3. The output of the TMCNC is then directed into the size measurement system.

Size Selection. A long DMA (TSI model 3071) is used for size selection. The flow rates of polydisperse aerosol and sheath air stream were 1.4 and 14 lpm, respectively. For this experimental setup, the DMA was practical for the selection of 6 nm and larger particles. It can be used for smaller sizes, but there are high diffusional losses in the inlet and tubing up to the top of the system. As part of the DMA, a radioactive charger with a source of ^{85}Kr is used to impart a low charge distribution. A potential concern in these experiments would be the production of particles through ion-induced nucleation. A ^{85}Kr source was used because earlier work had suggested it was less likely to produce additional particles.[22] Tests were run of the system with no generated particles to ensure that no ion-induced or homogeneous nucleation occurred at the vapor pressures of the working fluids used in these experiments.

To examine existence of generated carbon particles smaller than 6 nm, a SMEC and a nano DMA were used. The SMEC (SpectromPtre de Mobilité Electriqué Circulaire), the inward radial flow mobility analyzer, was developed by Pourprix and Daval.[23] Studies by Mesbah et al.[24] showed that it is effective at separating particles down to 1 nm. A nano DMA (TSI model 3085) can also separate down to 1 nm particles.[25] Using the SMEC with an ultrafine CNC (TSI model 3025 UCPC), size distributions of particles less than 6 nm were measured. These

TABLE 1: Contact Angles between Carbon and Working Fluids

Working fluid	Measured macroscopic contact angle (°) between carbon and the working fluid in air
DBP	7 ± 2
octadecane	0
octadecanol	15 ± 2
octadecanoic acid	8 ± 2

TABLE 2: Mixer Temperatures for Different Conditions of Saturator Temperature

saturator temperature (°C)	65	73.5	70.7
mixer temperature (K)	303.9	306.3	305.5

measurements show that particle concentrations for a given size varies greatly with the standard deviations in the particle concentrations in the size distributions were more than 100%. The nano DMA along with the CNC showed fluctuations of the particle concentrations from 0 to hundreds of particles/cm^3. Due to the variation, particle sizes less than 6 nm were not measured for heterogeneous nucleation analysis. This result means that the total number of particles detected will increase when carbon particles smaller that 6 nm are activated and nucleate droplets of working fluid that then grow to detectable sizes. This effect is a limitation to the measurements which is discussed below.

Particle Detection. The ultrafine CNC (TSI model 3025 UCPC) was used to measure number concentration of nanometer particles extracted from the DMA. The combination of the CNC and the DMA is the SMPS system used for obtaining size distributions. The TSI model 3025 enables the measurement of particles of 3 nm diameter and larger at concentrations of 10^{-3}–10^4 particles/cm^3.[26,27] The detection limit can reach 2−3 nm.[25,28−31]

For heterogeneous nucleation, the long DMA and the UCPC were used as an SMPS system. The SMPS system allows the measurement of particles 200 nm in size and smaller. To measure size distributions of grown particles of 200 nm or larger in size, a laser aerosol spectrophotometer-X (PMS LAS-X) was used. It has scanning range of 90 nm to 3.5 μm.[16,17]

Contact Angle. There was no information in the literature on the contact angles between carbon and working fluids, one of the important parameters in heterogeneous nucleation. Therefore, measurements of the contact angle were performed with a goniometer (Krüss Gmbh model ACAMS-40).

The four working fluids were dropped on a glass plate (Yissum Research Development Co.) on which carbon film was coated. Then, the macroscopic contact angles were measured. The measurements for DBP were performed at room temperature. For octadecane, octadecanol, and octadecanoic acid, the plate, the fluid, and the area in which the measurements were performed, were heated above their melting points by a heat lamp during the measurements as necessary. The melting points are 301, 331, and 343 K for octadecane, octadecanol, and octadecanoic acid, respectively. Due to the different size of the droplets of the fluids and the different temperatures, the measured contact angles varied by 2 degrees. The measured values are in Table 1.

Temperatures for Supersaturation Ratio. To obtain a supersaturation ratio for theoretical nucleation rates, temperatures in the mixer were measured using the digital thermometer mentioned before. The temperatures are listed with respect to the corresponding saturator temperatures in Table 2. For calculating saturation ratio, vapor loss in the mixer in the TMCNC must be considered. However, there is no method available to estimate the vapor loss in turbulent flow regime in the mixer. Thus, all of the supersaturation ratios were calculated based on saturation vapor pressure.

Properties of Working Fluids. Four working fluids were used in these studies and their physicochemical parameters are given in Table 3. These compounds were chosen to be similar in their thermodynamic properties, such as vapor pressure, while having differences in dipole moment and polarizability. Three of them have very similar molecular structure with the only difference being in the moiety at the end of the long CH chain.

TABLE 3: Physicochemical Properties of Working Fluids for Calculating Chemical Interaction Energy[a]

properties	DBP	octadecane	octadecanol	octadecanoic acid
molecular weight (g/mol)	278.3	254.5	270.5	284.5
boiling point (°C)	340.0	316.9	333.2	375.4
supersaturation ratio between 70 and 32 °C	84.9	42.7	112	82.7
monomer volume (m^{-3})	4.5×10^{-28}	5.5×10^{-28}	5.4×10^{-28}	5.4×10^{-28}
density at T(K) (kmol/m^3)		$A/[B^{\{1+(1-r/C)D\}}]$, where the coefficients are below:		
	A = 0.297	A = 0.241	A = 0.262	A = 0.264
	B = 0.251	B = 0.258	B = 0.265	B = 0.269
	C = 781.0	C = 745.3	C = 777.0	C = 799.0
	D = 0.374	D = 0.274	D = 0.327	D = 0.303
vapor pressure at T(K) (Pa)		$\exp(A + (B/T) + C \ln T + DT^E)$ with coefficients		
	A = 356.4	A = 129.2	A = 157.7	A = 124.7
	B = −24762	B = −15072	B = −18863	B = −16598
	C = −51.17	C = −14.47	C = −17.98	C = −13.56
	D = 0.039	$D = 4.16\times 10^{-18}$	$D = 1.50\times 10^{-18}$	$D = 3.16\times 10^{-18}$
	E = 1.00	E = 6.00	E = 6.00	E = 6.00
surface tension at T (K) (N/m)		$A(1 - T_r)^{(B+CT_r+DT_r^2+ET_r^3)}$, where $T_r = T/T_c$ with coefficients		
	A = 0.060	A = 0.057	A = 0.055	A = 0.054
	B = 1.219	B = 1.409	B = 1.234	B =1.147
critical temp (K)	781.0	745.3	777.0	799.0
dipole moment (Cm)	5.7×10^{-30}	0	5.4×10^{-30}	4.3×10^{-30}
polarizability volume (m^{-3})	4.6×10^{-29}	3.4×10^{-29}	4.2×10^{-29}	2.6×10^{-29}

[a] Equations and data are from physical and thermodynamic properties of pure chemicals (Daubert and Danner, 1996).

TABLE 4: Geometric Means and Standard Deviations of Log-Normally Fitted Modes

		1st mode		2nd mode		3rd mode		
working fluid	$P_{partial}$ (mPa)	d_g (nm)	σ_g	d_g (nm)	σ_g	d_g (nm)	σ_g	R^2
DBP	17.3	8.74	1.12	17.42	1.74	92.37	1.62	0.99
	25.9	8.23	1.17	24.82	1.49	118.16	1.78	0.97
	34.5	7.36	1.07	27.77	1.56	151.40	1.84	1.00
octadecane	51.7	6.78	1.04	35.09	1.78	187.67	1.66	1.00
	106	8.56	1.24					0.98
	159	7.90	1.16	81.79	2.46			0.98
	215	7.63	1.09	134.95	2.08			0.98
octadecanol	1.15	9.65	1.25					0.98
	2.28	8.97	1.27	23.91	1.49			0.98
	3.41	7.42	1.18	45.01	1.84			0.97
	4.55	6.80	1.07	73.33	2.04			1.00
octadecanoic acid	1.14	10.63	1.33	27.86	1.72			0.97
	2.27	8.08	1.21	51.82	1.95			0.98

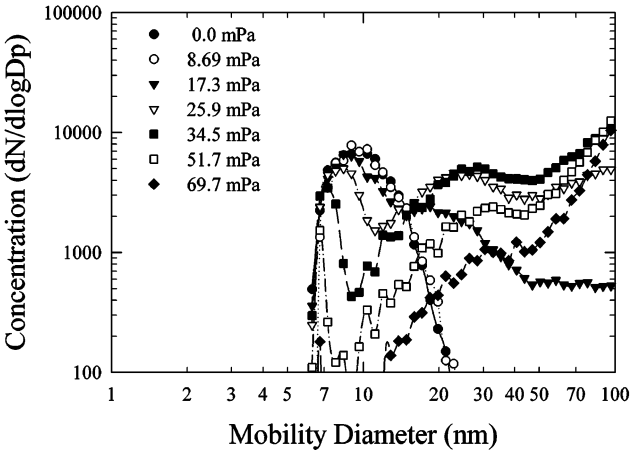

Figure 4. Particle size distributions with DBP at 73.5 °C of saturator temperature.

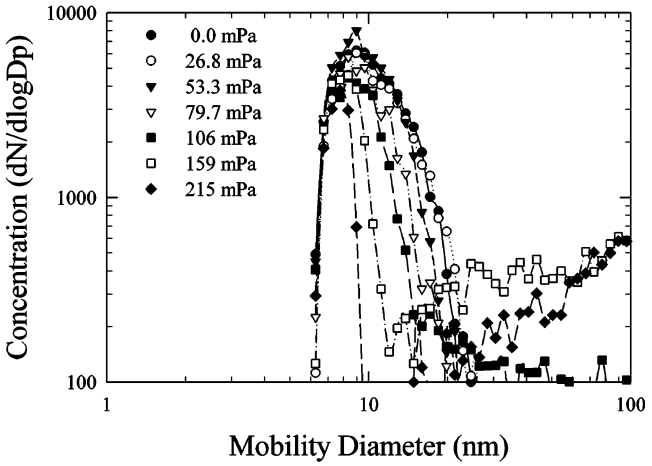

Figure 5. Particle size distributions with octadecane at 65 °C of saturator temperature.

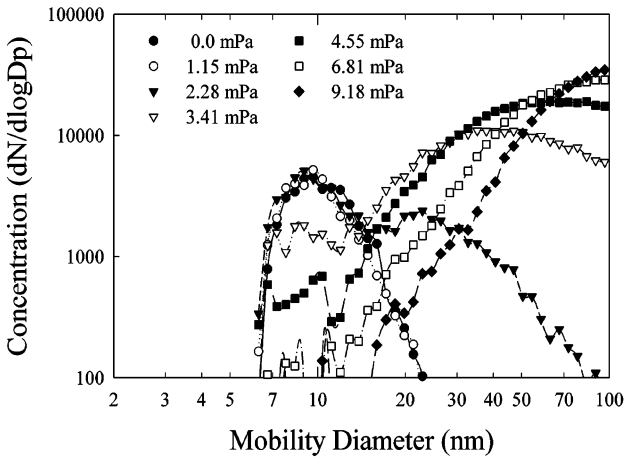

Figure 6. Particle size distributions with octadecanol at 65 °C of saturator temperature.

4. Experimental Procedure and Data Reduction

The generated carbon particles pass through the TMCNC for heterogeneous nucleation. Then, the particles are sorted by size in the DMA. The number concentration of the selected particles are measured in the CNC. Using the information of the particle sizes from the DMA and the corresponding number concentrations from the CNC, size distributions are obtained.

For a given condition of saturator temperature and flow rate, a series of size distribution measurements were performed. For each condition, at least 3 measurement series were made. Size distribution curves for selected conditions are fitted to a log-normal distribution. The conditions were chosen for calculating the experimental heterogeneous nucleation rate. The corresponding geometric means and standard deviations are presented in Table 4 with correlation coefficients, R^2. Almost all of the size distribution curves are well fit with a log-normal distribution. The smallest value of the squared correlation coefficient (R^2) is 0.97.

5. Results and Discussion

Figures 4 through 7 show measured size distributions. In Figures 4 to 7, the naught partial pressure, 0 Pa, denotes the condition where no working fluid was introduced into the mixer, which means that the filtered air passes only through the dry chamber. Thus, the measured size distributions at 0 Pa were just those of the carbon nuclei at each given temperature. Again, note that the presence of carbon particles smaller than 6 nm is probable, but they cannot be detected by the particle size analyzer. As the wet flow increases, the supersaturation ratio, S, rises to initiate heterogeneous nucleation and consequent particle growth.

Figure 4 shows the particle size distributions when DBP was used as a working fluid. At a saturator temperature of 68 °C, particle size distributions at 8.69 mPa of partial pressure are almost the same as the source distribution as shown in Figure 4. When the partial pressure was increased to 17.3 mPa, however, the particle size distribution differs from the source distribution. Comparing particle size distributions at 25.9 mPa of partial pressure and 0 Pa (carbon source particles), it can be seen that some of the 8.4 nm and larger diameter carbon particles

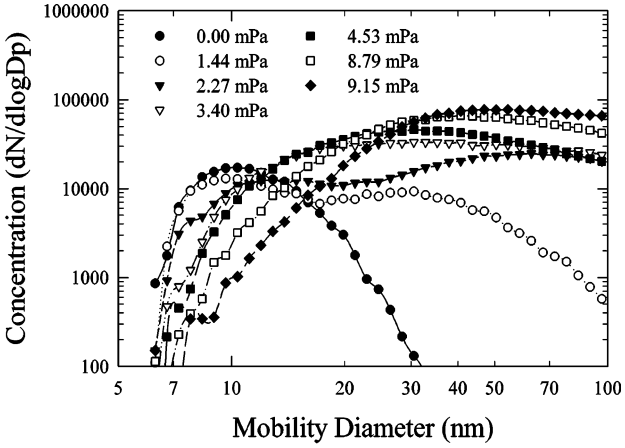

Figure 7. Particle size distributions with octadecanoic acid at 70.7 °C of saturator temperature.

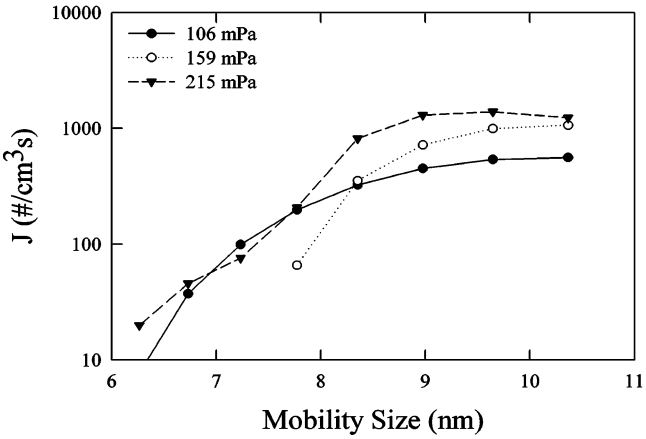

Figure 8. Heterogeneous nucleation rates with DBP at 73.5 °C of saturator temperature: lines with symbols denote experimental nucleation rates while series of only symbols are from calculations of Fletcher's theory.

are activated and grow to larger sizes, so that the concentration of the remaining (nonactivated) particles are fewer than that of carbon source particles in the same size range. Since the largest carbon particles are the first to be activated, the concentration difference becomes greater with increasing particle size, although carbon source particle concentrations above the size of 8.4 nm decrease rapidly with increasing partial pressure of DBP. It should be noted that for all runs above about 15 mPa, there appears a population of particles that was not present in the initial carbon particle distribution. These are the activated and grown droplets of working fluid. To measure the heterogeneous nucleation rate, it is not these large particles that are important, since we do not know from what size particle they formed. The depletion of the initial carbon particle population distribution is what is measured. This depletion is the concentration difference between the original source particle concentration and the final measured one at the higher partial pressure of working fluid.

The range of mobility diameters over which this measurement can be made is limited because, for a given supersaturation, there is a lower limit below which few carbon particles are activated and the population remains at the original value and an upper limit above which there are new particles generated by the activation of some of the smaller ones that have not grown out of the original measurement size range during passage through the CNC. The lower limit at 25.9 mPa is about 8.4 nm while the upper limit of measurement is at the minimum in the concentration versus mobility diameter at 10.5 nm. For all sizes larger than this, even though with a lower concentration that the initial concentration of carbon particles, the actual count is a combination of nonactivated initial carbon particles and activated smaller particles which grow into this size range. This means that the concentrations are contributed by particles that grow by vapor condensation after activation, as well as by inactivated particles. Because of the increased number of grown particles, the number concentration of the particles having 14.9 nm in diameter reaches almost the same concentration as that of the source particles. Then, the particle concentrations become greater than the source distribution in bigger particle sizes with a long tail.

At a partial pressures of DBP of 17.3 mPa or higher, the initial activation sizes decrease. The higher wet flow rate brings sufficient vapor into the processes of nucleation and growth, so that the grown particle size becomes larger. As shown in Figure 4, particle size distribution curves move to larger size and higher concentrations as the partial pressure rises by increasing vapor flow. The tail of high concentrations of larger particles was observed from the presumed large concentrations of initial nucleation below 6 nm where not observable in the initial source concentration profile at 0 mPa working fluid pressure.

When other working fluids, octadecane, octadecanol, and octadecanoic acid, are used, the first mode of the particle size distributions (Figures 5 through 7) for heterogeneous nucleation show the same activation patterns as DBP with respect to partial pressure, which increases with the wet flow rates. Initial activation size and particle concentration decreases as the wet flow rate increase.

Heterogeneous Nucleation. Using the concentrations from the fitted log-normal curves, each experimental heterogeneous nucleation rate at a given size and condition is calculated:

$$J(\#/\mathrm{cm}^3\, s) = \frac{(C_{@P=0\ \mathrm{Pa}} - C_{@P=x\ \mathrm{Pa}}) \times Q}{V_{\mathrm{mixer}}} \qquad (8)$$

where, $C_{@P=0\ \mathrm{Pa}}$ and $C_{@P=x\ \mathrm{Pa}}$ are the number concentrations (#/cm^3) when partial pressures are at 0 and x Pa, respectively, Q is the flow rate through the mixer, 1.4 lpm, and V_{mixer} is the volume of the mixer, 0.8 cm^3. When the size distributions show more than one mode, the second and the third modes, which are related to particle growth, were eliminated for investigating heterogeneous nucleation. The calculated experimental nucleation rates are shown in Figures 8 to 11. Figures 8, 10, and 11 show theoretical nucleation rates as well for comparison purpose.

Since octadecane has a macroscopic contact angle, θ, of 0 degrees and, the other two angles, ψ, and φ in Figure 2, are 0; i.e., the existing nucleus is placed inside of the liquid cluster with only one contact point as shown in Figure 12. Therefore, Fletcher's geometric factor, $f(m,x)$ needs to be corrected for octadecane.

When x ($= a/r^*$) >1, with $m(\cos\theta) = 1$ in eq 6, $g = (1 - x)$. Consequently, $f(m,x)$ becomes 0. Then, the Gibbs free energy in eq 5 also becomes 0. If $x = 1$, $g = 0$. Then, $f(m,x)$ in eq 6 is not valid.

Considering the case of x smaller than 1 as shown in Figure 12, $f(m,x)$ needs to be replaced by the ratio of the actual volume occupied by vapor to the critical cluster volume, $v(\theta) \equiv (r^{*3} -$

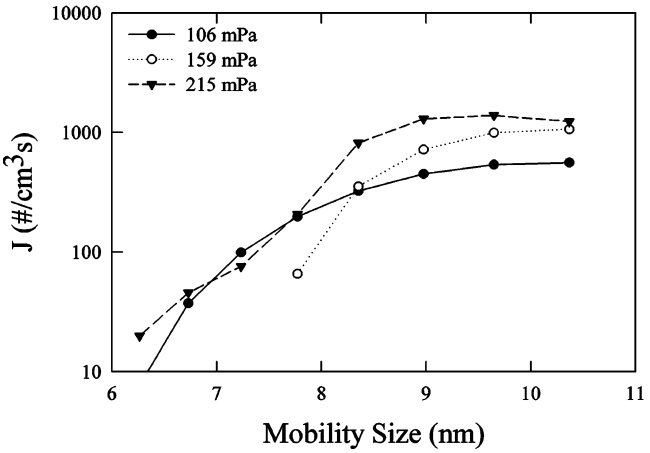

Figure 9. Experimental heterogeneous rates with octadecane at 65 °C of saturator temperature.

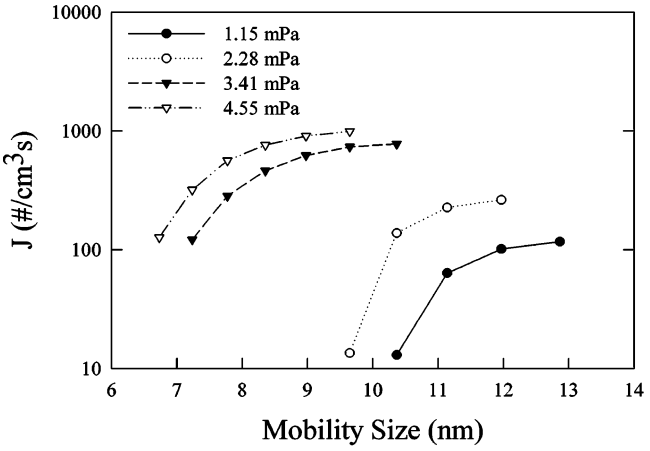

Figure 10. Heterogeneous nucleation rates with octadecanol at 65 °C of saturator temperature: lines with symbols denote experimental nucleation rates while series of only symbols are from calculations of Fletcher's theory.

$a^3)/r^{*3}$. In this case, instead of eq 5 the critical Gibbs free energy becomes

$$\Delta G^* = \frac{16\pi\gamma_{gl}{}^3}{3(\Delta G_v)^2}\upsilon(\theta) \qquad (9)$$

The critical Gibbs free energy for octadecane based on Fletcher's theory is 3.3×10^{-19} J or higher for a carbon particle, while values of k_BT are about 4.2×10^{-21} J. Thus, the exponential term, $\exp(-\Delta G^*/k_BT)$, in eq 7 becomes 1.0×10^{-34} or smaller. Since the calculated prefactor

$$\frac{s(\theta)}{\sqrt{\upsilon(\theta)}}\sqrt{\frac{2\Omega^2\gamma}{\pi m_1}} f_{1\,\mathrm{het}}\, f_1\{1 + (n^*_{\mathrm{hom}})^{-1/3}\}^2 \qquad (10)$$

in the heterogeneous nucleation rate equation does not exceed 10^7 particles/cm^3 s, the calculated nucleation rate is 3.8×10^{-28} particles cm^{-3} s^{-1}, which is close to 0 particles cm^{-3} s^{-1}. This calculation suggests that heterogeneous nucleation is almost impossible. However, the experiments show that particles were activated as seen in Figure 9.

For DBP, most of the Gibbs free energy values calculated by Fletcher's theory fall in the range of 10^{-20} and 10^{-21} J, which gives values of nucleation rates of 1.4×10^4 and 1.2×10^5 particles cm^{-3}s^{-1}, respectively. When the supersaturation ratio is higher than 5, i.e, for the conditions of 25.9, 34.5, and 51.7 mPa, the calculated nucleation rates by Fletcher are match well with the experimental values as shown in Figure 8. There are about 2 orders of magnitude difference between the theoretical and the experimental nucleation rates that could be caused by uncertainties in the prefactor. When S is less than 5, Fletcher's theory shows large differences from the experimental results in Figure 8 (for the condition of 17.3 mPa).

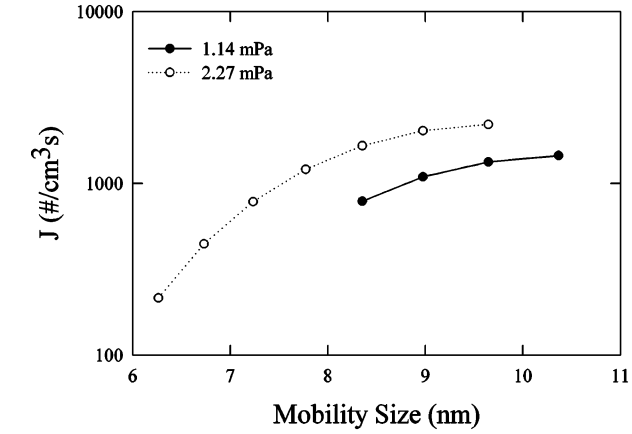

Figure 11. Heterogeneous nucleation rates with octadecanoic acid at 70.7 °C of saturator temperature: lines with symbols denote experimental nucleation rates while series of only symbols are from calculations of Fletcher's theory, and only lines are ratios of the chemical interaction to Fletcher's heterogeneous nucleation energy.

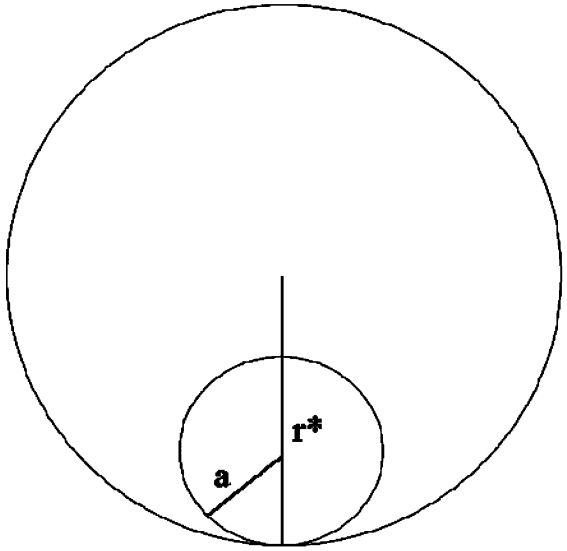

Figure 12. Schematic view of critical liquid cluster containing a preexisting nucleus inside: θ, ψ, and φ are 0.

When octadecanol and octadecanoic acid vapor were used for heterogeneous nucleation, the theoretical results are well matched with the experimental results for most conditions as shown in Figures 10 and 11. The differences caused by the prefactor are even smaller than those for DBP with the differences in the range of 1 order of magnitude.

For calculating heterogeneous nucleation, carbon nucleus and monomer shapes were assumed to be spherical. Examination of this assumption may help explain the observed discrepancy between the experimental results and the theoretical prediction. The shape of carbon particles and monomers was assumed to be spherical. di Stasio et al.[32] suggested that carbon particles generated by combustion processes are likely to have a fractal shape. This shape may give more contact area than a spherical shape. Since a vapor molecule has a long chain of C−C bond, it may have steric hindrance with other molecules when it makes

TABLE 5: Total Number Concentrations of Grown and Source Particles

working fluid	$P_{partial}$ (mPa)	total number concentration (#/cm^3) of source particles	total number concentration (#/cm^3) of inactivated and grown particles	concentration (#/cm^3) from SMPS	concentration (#/cm^3) from LAS-X
DBP	17.3	1933	2738	1447	23
	25.9		5790	3315	1592
	34.5		11763	4665	6807
octadecane	51.7		20001	2980	16962
	106	1508	1179	102	8
	159		1518	398	364
	215		6519	184	5960
octadecanol	1.15	1129	1135	50	0
	2.28		2033	925	0
	3.41		7865	6633	598
	4.55		12205	10295	1869
octadecanoic acid	1.14	4741	9227	5141	48
	2.27		18665	14053	3992

TABLE 6: Physical Properties of Water[a]

property	value or equation with coefficients
molecular weight(g/mol)	18.0
density (kmol/m^3) at T (K)	$A + B(1 - T_r)^{0.35} + C(1 - T_r)^{2/3} + D(1 - T_r) + E(1 - T_r)^{4/3}$ A = 18.06, B = 25.31, C = 66.17, and D = −50.21
vapor pressure (Pa) at T (K)	$\exp(A + B/T + C \ln T + DT^E)$ A = 73.65, B = −7258.2, C = −7.30, D = 4.17×10^{-6}, and E = 2
surface tension (N/m) at T (K)	$A(1 - T_r)^{(B+CT_r+DT_r^2+ET_r^3)}$ A = 0.1855, B = 2.717, C = −3.554, and D = 2.047
critical temperature (K)	647.13

[a] Equations and Data are from physical and thermodynamic properties of pure chemicals (Daubert and Danner, 1998).

contact with a carbon particle. Therefore, the actual number of molecules having direct contact with a carbon particle could be different from the calculated. It will affect the geometrical factors, $f(m,x)$ and $\upsilon(\theta)$ in eqs 5 and 9, respectively. To obtain the actual number concentration affecting the geometrical factor, further studies are needed.

Particle Growth. As shown in Figures 4 through 7, the particle size distributions have a second and sometimes a third mode. The grown particle sizes have diameters of the order of 100 nm as summarized in Table 4. For octadecane, Figure 5 shows that few particles grow into the particle size range of 20 nm to 100 nm. In the case of octadecanol and octadecanoic acid as shown in Figures 6 and 7, respectively, the size distributions show that large particles have even higher number concentrations than those with DBP vapor. This increase may be the result of the interactions between hydrophilic functional groups, −OH and −COOH, and large amount of water vapor produced by the combustion process for particle generation.

When DBP is used for working fluid, the grown particles show two modes in the size distributions in Figure 4. The second mode is not found with octadecanol and octadecanoic acid as shown in Figures 6 and 7. The third mode with DBP is in the size range of greater than 35 nm where the second modes with other vapors were found. For this reason, further study of this particle growth is required.

For the second and/or third modes, i.e., for grown particle size distributions, shown in Figures 4 through 7, geometric means and the number concentrations of the particles tend to increase as the wet flow rates were raised, which results in introducing more vapor into the mixer at a given temperature. For the case of octadecane, however, this relationship is not obvious.

All of the activated and grown particles were measured in the size range of up to 3.5 μ. The number concentrations measured using SMPS for smaller particles, and LAS-X for larger particles than 100 nm in size are shown in Table 5 along with the number concentration of source carbon particles. Table 5 shows that the total number concentrations of the remaining (inactivated) and grown particles are higher than that of carbon source particles with an exception of 106 mPa of octadecane vapor pressure. The higher number concentration may be the result of fluctuations in the number concentration of carbon source particles, especially at low partial vapor pressure of each vapor. However, at high partial vapor pressure, the measured total number concentrations are more than 5 times higher than the carbon source particle concentrations. This means that some particles were generated from additional nucleation and/or growth processes other than those related to carbon particles of 6 nm or larger, and contribute to the total concentrations.

To examine whether any new particles could be generated by unary and/or binary nucleation, nucleation rates were calculated. For the unary nucleation of the working fluids' vapor, the calculated Gibbs free energies are too high: the lowest energies for DBP, octadecane, octadecanol, and octadecanoic acid are, respectively, 1.1×10^{-18}, 3.3×10^{-18}, 4.0×10^{-19}, and 5.3×10^{-19} J while k_BT is about 4.0×10^{-21} J. The consequent nucleation rates are almost 0. Thus, unary nucleation based on theory is not likely to occur.

Next, binary nucleation of the working fluid vapor and water vapor, produced by combustion processes, was examined. To use the conceptual framework of Kulmula and Viisanen,[33] it is necessary to determine the virtual monomer volume:

$$\Omega = (1 - X)\Omega_a + X\Omega_b \tag{11}$$

where Ω_a and Ω_b are, respectively, a working fluid monomer and a water monomer volume, and X is the water vapor fraction. Parameters for the calculations, molecular weight, density, vapor pressure, and surface tension of water, are provided in Table 6. Water vapor pressure is 3.5 kPa while vapor pressure of working fluids is at most 4.5×10^{-2} Pa. Although Ω_a is about 15 times Ω_b, the number of water vapor molecules in the virtual monomer

TABLE 7: Summarized Data for Calculating Sublimation Vapor Pressure

fluid	vapor pressure (Pa) at melting point	melting point (K)	ΔH_{sub} (kJ/mol)[a]
octadecane	0.0337	301.33	153.0
octadecanol	0.0280	331.05	187.4
octadecanoic acid	0.0563	342.75	167.0

[a] Data are from the website of NIST (http://webbook.nist.gov/cgi/cbook.cgi). All of the other data are from physical and thermodynamic properties of pure chemicals (Daubert and Danner, 1998).

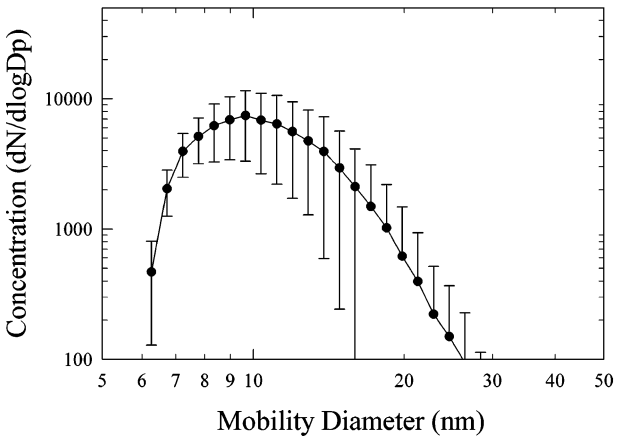

Figure 13. Carbon source particle size distribution.

is so dominant that water vapor fraction is close to 1. Thus, the binary nucleation is equivalent to homogeneous nucleation of water.

The aerosol stream was saturated with water vapor at 300 K. Then, it cooled to 293.15 K in the condenser of the TMCNC. Since S is only 1.5, the corresponding Gibbs free energy is 5.3×10^{-18} J while k_BT is 4.0×10^{-21} J. Therefore, unary nucleation of water vapor is not possible.

For octadecane, octadecanol, and octadecanoic acid, the sublimation vapor pressure P (Pa) at a given temperature T (K) is calculated with the Clausius−Clapeyron equation:

$$p = p^* \exp\left\{-\frac{\Delta H_{sub}}{R}\left(\frac{1}{T} - \frac{1}{T^*}\right)\right\} \qquad (12)$$

where p^* is the saturation vapor pressure at melting point T^*, ΔH_{sub} denotes the enthalpy of sublimation, and R is the gas constant. Saturation vapor pressures of the working fluids at their melting points and the enthalpies of vaporization are summarized in Table 7.

Since neither theoretical unary nucleation of the working fluids or water is likely to occur, the observed nucleation can be explained only by consideration of additional particle source. As mentioned earlier, particles smaller than 6 nm were detected although the particle concentration values had more than 100% standard deviation. As shown in Figure 13, average standard deviation of the measured carbon source particle concentrations using model 3071 DMA are approximately 50% over all of the size range with 73% for 6.0 nm particles. With extrapolating error bars to smaller particles, 6.0 nm or smaller particles are likely to exist. These particles may be the additional source.

When DBP, octadecanol, and octadecanoic acid are used for working fluids, the grown particle size and number concentration gradually increases with partial vapor pressure. Figure 14 shows the ratio of fluid's mass accumulated on particles to mass of the vapor delivered into system. If the working fluids are the only source of the vapor supplied for heterogeneous nucleation and, especially, for particle growth, then the accumulated vapor fraction becomes constant at higher pressures because the supersaturation is substantially higher than critical supersaturation, and the growth then depends linearly on pressure of the condensable vapor.[31] Above a certain vapor pressure, Figure 14 shows that the accumulated liquid ratio increases rapidly with increasing pressure. The ratio reaches up to 0.8. Concerning vapor loss caused by condensing on the condenser wall, it is concluded that water vapor is likely to be involved in the growth process.

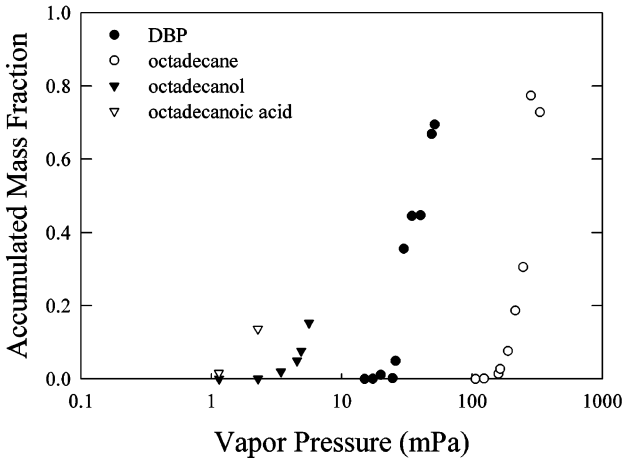

Figure 14. The fractional ratios of each working fluids mass accumulated on carbon particles to total mass of each vapor pressure delivered into system with respect to partial vapor pressure.

DBP, octadecanol, and octadecanoic acid have at least one hydrophilic functional group, ketone, hydroxyl, and carboxilic acid group, respectively. Water vapor could interact with these groups. There is a considerable amount of water vapor, 1.2 kPa in pressure, available that can directly interact with the condensed fluids. For octadecane, these interactions are not likely because octadecane is a hydrophobic substance. To qualify and quantify the hypotheses in this study, further studies will be necessary.

6. Conclusions

Experimental heterogeneous nucleation rates on combustion carbon particles were measured for selected working (condensing) fluids using a TMCNC and compared with the theoretical rates based on Fletcher's (classical) heterogeneous nucleation theory. The experimental rates were found to differ from the theoretical values, with the differences being more than 10 orders of magnitude for DBP and hundreds of orders of magnitude for octadecane. Consideration of homogeneous and binary nucleation at the low supersaturations of this study cannot explain the observed nucleation rates. We cannot explain the gap between the experimental measurements and the Fletcher theory for octadecane. There may be nanoscale interactions, activation of smaller-than-expected-particles or multiple nanoparticle interactions that occur between the organic species, carbon particles, and working vapor. These speculations do not explain the discrepancy between theory and experiment. Further studies will be necessary to examine these hypotheses.

Acknowledgment. This research has been supported by a grant from the U.S. Environmental Protection Agency's Science to Achieve Results (STAR) program. Although the research described in the article has been funded wholly by the U.S. Environmental Protection Agency's STAR program through

grant R826654, it has not been subjected to any EPA review and therefore does not necessarily reflect the views of the Agency, and no official endorsement should be inferred. We acknowledge the useful discussions of these results with Michael Anisimov and Dr. Vladimir Smorodin of Clarkson University.

References and Notes

(1) Seaton, A.; MacNee, W.; Donaldson, K.; Godden, D. *Lancet* **1995**, *345*, 176−178.
(2) Peters, A.; Wichmann, H. E.; Tuch, T.; Heinrich, J.; Heyder, J. *Am. J. Respir. Crit. Care Med.* **1997**, *155*, 1376−1383.
(3) Kim, S.; Jaques, P. A.; Chang, M.; Froines, J. R.; Sioutas, C. *J. Aerosol Sci*. **2001**, *32*, 1281−1297.
(4) Kim, S.; Jaques, P. A.; Chang, M.; Barone, T.; Xiong, C.; Friedlander, S. K.; Sioutas, C. *J. Aerosol Sci*. **2001**, *32*, 1299−1314.
(5) Sioutas, C.; Koutrakis, P. *Aerosol Sci. Technol*. **1996**, *25*, 424−436.
(6) Fletcher, N. H. *J. Chem. Phys.* **1958**, *29*, 572−576.
(7) Volmer, M. and Weber, A. *Z. Phys. Chem*. **1926** *119*, 277−301.
(8) Wu, D. T. *Solid State Phys.* **1997**, *50*, 37−187.
(9) Volmer, M. *Z. Elektrochem*. **1929**, *35*, 555−561.
(10) Fletcher, N. H. *The Physics of Rainclouds*; Cambridge University Press: Cambridge, 1969.
(11) White, L. R. *J. Chem. Soc., Faraday Trans. 1* **1977**, *73*, 390−398.
(12) Friedlander, S. K.; Lippmann, M. Revising the Particulate Ambient Air Quality Standard. *Environ. Sci. Technol.* **1994**, *28*, 148A−150A.
(13) Helsper, C.; Niessner, R. *J. Aerosol Sci.* **1985**, *16*, 457−461.
(14) Porstendörfer, J.; Scheibel, H. G.; Pohl, F. G.; Preining, O.; Reischl, G.; Wagner P. E. *Aerosol Sci. Technol.* **1985**, *4*, 65−79.
(15) Kesten, J.; Reineking, A.; Porstendörfer, J. *Aerosol Sci. Technol*. **1991**, *15*, 107−111.
(16) Kousaka Y.; Okuyama K.; Niida T. In *Aerosols*; Liu, B., Pui, D., Fissan, H., Eds.; Elsevier: New York, 1984; 51−54.
(17) Madeline, G.; Metayer, Y. *J. Aerosol Sci.* **1980**, *11*, 358.
(18) Hopke, P. K.; Lee, D.-W.; Mavliev, R.; Wang, H.-C. In *Nucleation and Atmospheric Aerosols 2000: 15th International Conference*; Hale, B. N., Kulmala, M., Eds.; Elsevier Science Ltd.: Oxford, 2000; 139−142.
(19) Mavliev, R.; Hopke, P. K.; Wang, H.-C.; Lee, D.-W. *Aerosol Sci. Technol*. **2001**, *35*, 586−595.
(20) Lee, D.-W. Ph.D. Thesis, Clarkson University, 2002.
(21) Li, W.; Hopke, P. K. *Aerosol Sci. Technol.* **1993**, *19*, 305−316.
(22) Leong, K. H.; Hopke, P. K.; Stukel, J. J. *J. Aerosol Sci.* **1983**, *14*, 23−27.
(23) Pourprix, M.; Daval, J. In *Aerosols: Science, Industry, Health and Environment*, Proc. 3rd International Aerosol Conf., Kyoto, Japan, vol. II. Masuda, S., Takahashi, K., Eds.; Pergamon Press: Oxford, 1990.
(24) Mesbah, B.; Fitzgerald, B.; Hopke, P. K.; Pourprix, M. *Aerosol Sci. Technol*. **1997**, *27*, 381−393.
(25) Chen, D.-R.; Pui, D. Y. H.; Hummes, D.; Fissan, H.; Quant, F. R.; Sem, G. J. *J. Aerosol Sci*. **1998**, *29*, 497−509.
(26) Stolzenburg, M. R.; McDermott, W. T.; Schwartz, A. *J. Aerosol Sci*. **1988**, *19*, 1015−1018.
(27) Stolzenburg, M. R.; McMurry, P. H. *Aerosol Sci. Tech*. **1991**, *14*, 48−65.
(28) McDermott, W. T.; Ockovic, R. C.; Stolzenburg, M. R. *Aerosol Sci. Technol*. **1991**, *14*, 278−287.
(29) Okuyama, K.; Kousaka, Y.; Motouchi, T. *Aerosol Sci. Technol*. **1984**, *3*, 353−366.
(30) Mavliev, R.; Wang, H.-C. *J. Aerosol Sci.* **2000**, *31*, 933−944.
(31) Mavliev, R. *Atmos. Res.* **2002**, *62*, 303−314.
(32) di Stasio, S.; Konstandopoulos, A. G.; Kostoglou, M. *J. Colloid Interface Sci.* **2002**, *247*, 33−46.
(33) Kulmala, M.; Viisanen, Y.; Laaksonen, A. *J. Aerosol Sci.* **1991**, *22*, S97−S100.